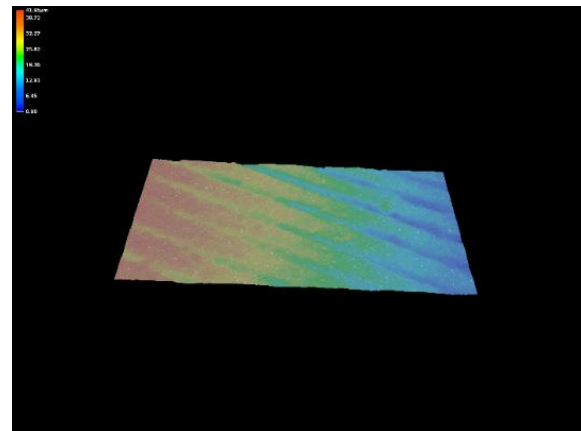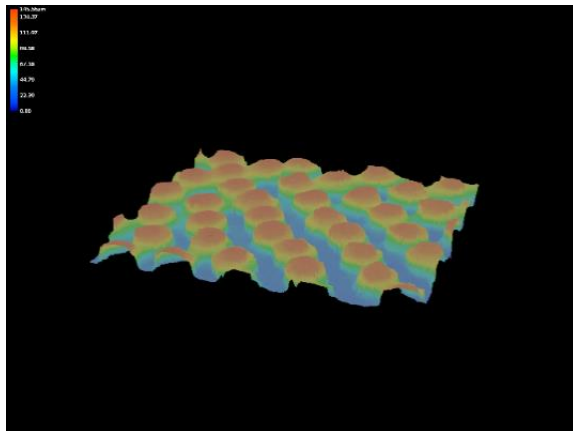**Embry-Riddle Aeronautical University**

Ceramic Research Advancement Technology at Embry-Riddle (C.R.A.T.E.R.)

Miquela Smith, Aerospace Engineering, Undergraduate; Maximus Mendez, Aerospace Engineering, Undergraduate; Justin Astacio, Aerospace Engineering, Undergraduate; Caleb Thompson, Aerospace Engineering, Undergraduate; Zeba Momin, Aerospace Engineering, Undergraduate; Luizandrei E. Galanida, Aerospace Engineering, Undergraduate; Tristan Ahuna, Aerospace Engineering, Undergraduate; Joanna Jose Fnu, Aerospace Engineering, Undergraduate; Avi Waghray, Aerospace Engineering, Undergraduate

Faculty Advisor: Dr. Seetha Raghavan

TABLE OF CONTENTS

Nomenclature

Al_2O_3 =   Alumina

CRATER =   Ceramic Research Advancement Technology at Embry-Riddle

DIW   =   Direct Ink Writing

FDM   =   Fused Deposition Modeling

GEO   =   Geostationary Equatorial Orbit

HLS   =   Human Lander System

HVOF   =   High-Velocity Oxygen Fuel

JAXA   =   Japan Aerospace Exploration Agency

LCM   =   Lithography-based Ceramic Manufacturing

LEO   =   Low Earth Orbit

LSMO   =   Lanthanum Strontium Manganite Oxides

NASA   =   National Aeronautical and Space Administration

PDMS   =   Polydimethylsiloxane

PSI   =   Plume Surface Interaction

SPS   =   Spark Plasma Sintering

USPL   =   Ultra Short Pulse Laser

WC-Co =   Tungsten Carbide Cobalt

ZrO_2 =   Zirconia

Major Objectives & Technical Approach

Objectives

- Determine the efficacy of the coating the Tungsten Carbide Cobalt coating to resist lunar regolith damage.

- Evaluate the improved adhesive resistive properties of the two surface modifications applied to the coating.

Technical Approach

- Research the different mitigation methods utilized in industry and develop a new innovative solution.

- Manufacture buttons of WC-Co coatings utilizing Cold Spray

- Manufacture buttons of Alumina (Al_2O_3) utilizing ceramic 3D printing

- Test and analyze sample buttons through various processes.

Key Design Details & Innovations of the Concept

Design Details

- Manufacturing method of WC: Cold Spray

- Bio-Inspired Surface Modification: Lotus Leaf and Beetle Patterns

- Manufacturing method of Surface Modifications: 3D Printed Ceramic Tiles

Innovations

- This coating enhanced with bio-inspired surface modifications effectively minimizes the adhesion of lunar regolith to these improved surfaces on the Human Lander Systems.
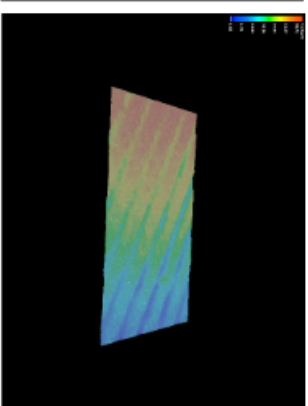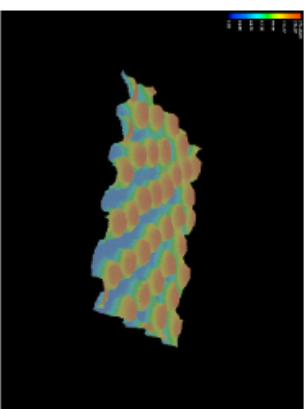
Costs and Schedule for Tests and Analysis

Cost

- Cold Spray WC-Co Button Samples: $4,925.00

- LSP-1D Regolith Simulant: $204.23

Schedule

- Manufacture sample coating buttons and 3D-printed ceramic tiles

- Conduct Tap Tap Experiment on 3D Printed Ceramic Tiles

- Conduct Grit Blaster Experiment on sample button of WC coatings

1   Problem Statement

Lunar regolith poses significant risks to the structural integrity of lunar human lander systems (HLS) due to its abrasive properties, cohesion, and prevalent adhesion. Lunar regolith affects the longevity and performance of equipment on the moon's surface. As a result, mitigating dust adhesion and abrasion by enhancing the structural integrity of the human lander system is critical to NASA's Artemis program. Highlighted by previous lunar missions, the comprehensive dust contamination caused numerous issues across vital systems for the HLS. These dust coatings caused significant wear on equipment, tools, and surfaces due to the fine and irregular edges of the dust particles. The persistent behavior of lunar regolith to adhere to surfaces results in lunar regolith compromising thermal control surfaces, seals, mechanisms, and surrounding structures. The development of effective lunar regolith mitigation strategies is necessary to enhance HLS asset safety and integrity.

Numerous concepts are currently being investigated and developed to mitigate the impact of lunar regolith. These approaches are classified broadly by the utilization of energy or mechanical processes to achieve this goal. C.R.A.T.E.R.'s proposed solution is a passive mitigation method, characterized by a ceramic coating augmented with a biomimetic surface pattern. The proposed ceramic coatings will enhance the surfaces on the HLS to mitigate lunar regolith dust abrasion and adhesion. Tungsten-Carbide and Alumina (Al_2O_3) are exceptionally durable and wear-resistant materials that will limit the abrasive effects posed by lunar regolith. By modifying the external surface of the Tungsten-Carbide using bio-inspired patterns, the coating can be altered to hinder dust adhesion or abrasion. To actualize this solution, C.R.A.T.E.R. investigated various approaches to develop this coating.

Our techniques to develop our coatings incorporated both additive and subtractive approaches. The first approach to develop our coating utilized a Cold Spray deposition method to coat a stainless-steel substrate with WC-Co. The surface of this coating was enhanced by etching biomimetic-inspired patterns using laser ablation. The second approach that was pursued used Lithography-based Ceramic Manufacturing (LCM) with Alumina. This additive manufacturing process allowed for the surface of our coating to be modified with biomimetic-inspired patterns. Out of various biomimetic patterns, the Lotus Leaf and Beetle were chosen for their ability to yield higher durability and hydrophobic properties.

When determining the appropriate approach for mitigating lunar regolith's effects, a trade study was developed to assess the various passive mitigation options (See Table 3). Following this structured approach, an opportunity was realized with surface coatings, which our team decided to pursue. The trade study can be viewed in the appendices.

2   Project Description

2.1   Justification of Assumptions

As previously mentioned, the landing spot of the HLS is the Lunar South Pole. Thus, the WC-Co coating will have to account for the temperature changes that the human lander will endure during the expedition. The expected extreme temperature ranges are between 50ºK to 221ºK (-223ºC to 494ºC). [24] The importance of determining the extreme temperature ranges of the South Pole for design constraints and guidelines is to verify the reliability of tungsten carbide in these temperatures' extremes. The high-end temperature of WC-Co can perform its positive characteristics such as dust abrasion, hardness, and toughness at 510ºC [25]. The coating will then be able to survive in the extreme high-end temperature of

the lunar south pole. The extreme low-end temperature will be proven through future testing. The coating can/will maintain its physical properties through the extreme temperature ranges of the lunar surface, thus the next dilemma the coating must face is the impact of micrometeoroid/debris coming from outer space.

The first approach to categorizing the overall impact Micrometeoroid/debris impacts will have on the WC-Co is to further understand the issue. Micrometeoroids/debris pose a threat to spacecraft and human spacesuits due to the speed at which they travel at. On average, a micrometeoroid/debris can travel at a high velocity of 7-15 km/hr [26]. Thus, the coating must be resilient to these micrometeoroids/debris impact on the lunar surface. The frequency of micrometeoroid/debris impact made on the lunar surface was also considered. There are around 10^6 kg of micrometeoroids that impact the lunar surface per year [27]. The WC-Co is expected to remain vigilant and is known for its high impact resistance, thus allowing the coating to be successful in dealing with the impacts of the micrometeoroids/debris. The coating also has other properties and surface modifications to reduce the lunar regolith dust impact caused by the small micrometeoroid/debris impacts near the lander.

The main obstacle that arises from landers leaving Earth and traveling through LEO and GEO is being exposed to atomic oxygen. Atomic oxygen is set to cause "erosion and chemical degradation" of material/substrates. In this case, the concern for these effects will be the most determinantal to the coating surface. When finding the true impacts of oxidation of the coating it can be difficult to assess [28]. This results in many effects that the tungsten carbide coating will undergo due to the atomic oxygen. As also mentioned in [28] the effects can result in either positive effects such as increased wear resistance or negative effects such as degradation in mechanical properties. Another factor to consider is the expected duration of the mission will be taken on the moon's surface, which in comparison to the atomic oxygen located at LEO shows less concern on the lunar surface. This, however, leads to the coating's expected exposure to UV and solar radiation from the moon's surface.

The moon has little to no atmosphere, thus it is exposed to a much greater deal of UV and solar radiation. For a comparison of solar radiation, the earth experiences around 2.4 millisieverts (mSv), while the moon experiences around 110-360 mSv [29]. This explains the overall environment that the coating will have to sustain on the lunar surface. The coating will also be exposed to solar irradiation on the lunar surface. This value is equivalent to the earth value of 1361 W/m^2 [30]. The coating must be able to handle these solar conditions.

When developing this solution to mitigating the lunar dust adhesion to the HLS, the assumption that there would be no preexisting infrastructure on the moon supporting the landing of HLS on the surface of the moon was made. This passive solution is intended to be sustainable and reusable for various lunar landing missions as the application of the coating is a preflight manufacturing process applied to various surfaces of the lander. Traveling across the lunar surface as well as during landing operations causes the surface of the moon to stir and create dust plumes. The intended purpose of this coating is to prevent adhesion and damage to the outer surfaces of the lunar landing when dust plumes accumulate during touch down. Dust contamination is a major concern when observing the potential health hazards astronauts will be exposed to during moonwalks. Minimal additional risks are imposed on the astronauts by the shedding of the WC-Co coating as the major concern is the tracking of lunar dust particles into the lunar habitats, contaminating them. These dust particles pose respiratory health hazards to the astronauts, but the amount of WC-Co will be minimal compared to the amount of lunar dust and other fine particle present on the lunar surface.

2.2　　　Revisions to Proposed Solution

From the initial development of this proposed mitigation method to the new changes and additions to the solution, much research and development has been conducted. The first concept idea involved the utilization of the High-Velocity Oxygen Fuel method of deposition for manufacturing the WC-Co sample button. However, after further researching different deposition methods and discussing the feasibility of manufacturing samples for testing, the deposition method chosen to create the button sample was Cold Spray. Although both HVOF and Cold Spray are thermal deposition methods they differ in the range of specifications. Both thermal deposition methods have high deposition efficiencies and have high densities, making them more resistant to wear over time. Cold Spray is more limited in the materials that can be processed when compared to the materials HVOF can process. However, Cold Spray is a cleaner process that does not use any methods of chemical heating or toxic exhaust.

In addition to the lotus leaf, research was conducted to observe various other bio-inspired surface modifications to evaluate the effectiveness of these modifications in preventing the adherence of the lunar regolith. One such biomimetic-inspired pattern that has been seen in nature that has properties limiting either abrasion or adhesion is the beetle pattern inspired by the Scarabaeus (Desert) Beetle. It was chosen as an additional surface modification as many studies outline its effectiveness in sandy and dusty environments with its enhanced wear resistance. For example, a study on the structure of a desert beetle's shell adapted to a hardened AISI M2 steel substrate coated with NiCrBSi and textured to follow the beetle's pattern, has revealed enhanced wear behavior [11].

Initially LHS-1D and LMS-1D were the chosen simulants for testing due to their particle size (0.04µm-30µm) and an assumption that either LHS-1D and LMS-1D would have a mineralogical makeup close enough to the South Pole regolith that the data would not be affected. However, after conversing with Exolith, the lab manufacturing these simulants, the LSP-1D (Lunar South Pole) simulant was found to be the most accurate simulant. It maintained the same particle size as LHS-1D and LMS-1D, while also being manufactured to accurately portray the makeup of regolith from the Lunar South Pole.

The final addition to this mitigation method is the implementation of 3D printing of ceramic tiles. Ceramic 3D printing was discovered when researching how to apply the lotus leaf (and beetle pattern) designs to the surface of the WC-Co coating. The team then reached out to the company Lithoz to create the surface modifications. The team modeled the surface modification of the lotus leaf and the beetle pattern in AutoCAD and with these models, Lithoz was able to 3D print them using Alumina. These samples will be used in adherence testing. Through research and concept adaptations this paper strives to demonstrate the feasibility of the implementation of this innovative mitigation method for future lunar lander missions.

The proposal contained a calculation error regarding the mass per square centimeter of the WC-Co coating. The number provided was the density, 14.9 g/cm^3, rather than the mass for a 250-micron thick coating. Correctly, using the formula for density, where the thickness (height) is 250 microns (0.025 cm), and the area (length x width) is 1 cm^2, the mass per square centimeter is 0.3725 grams. This confirms that the mass per square centimeter is 1/40th of the provided density value. Similarly, mentioned under the cost estimates section, the cost estimate uses a thickness of 0.01 inches, which is approximately 254 microns. Using this thickness then, the mass per square centimeter is 0.37846 grams. To prevent further errors, calculations were meticulously performed by hand, ensuring correct inputs. Detailed calculations are provided in Appendix 6.2.1.

2.3   Innovative Technological Approach

The team's proposed solution utilizes several innovative technologies to accomplish the proposed solution. Both the coating material Tungsten Carbide Cobalt and the Cold Spray deposition method used to apply it are innovative as they have not been used in the team's capacity. Along with this base, bio-inspired patterns are a new field of research with much to be developed. These patterns have never been manufactured on a large scale, but through testing and evaluation, the technologies utilized on this project can be further developed to meet this need to mitigate the effect of plume surface interactions (PSI).

2.3.1   WC-Co Coating

The material tungsten carbide was chosen as the proposed coating material for several reasons. First, is its high hardness (Vickers Number of 2,600) and melting point (5,200°F). These properties will allow the material to withstand the adverse effects of PSIs and the general lunar surface. This ceramic also exhibits a Young's modulus of 530 GPa with a density of 15.6 g/cm^3. The material tungsten carbide was chosen as the proposed coating material for several reasons. The deposition method chosen to create sample buttons of the WC-Co ceramic coating was Cold Spray and was manufactured by VRC Metal Systems. The Cold Spray deposition method is a Solid-State process that utilizes kinetic energy to deposit the material onto the substrate instead of using thermal energy as seen in HVOF. The process by which the material is deposited utilizes a high-pressure carrier gas, Nitrogen or Helium, which is electrically heated and used to accelerate the metal powers through a supersonic nozzle. The metal powers used in manufacturing the sample buttons was WC-Co. The unique aspect of Cold Spray is the carrier gas is heat below the melting temperature of the metal powers, so the depositing of material uses more kinetic energy, lowering the potential for the substrate material to warp. It can be observed that the microstructure of the metal powder before application to the substrate is very similar to the produced metal coating. When discussing the feasibility of VRC creating our samples the company proposed many different solutions to help the team. For the most cost-effective and time efficient manufacturing a few decisions to account for the limited time range for manufacturing, shipping, and testing. The substrate material used to create the samples was Stainless Steel as VRC already had the means to manufacture the coatings using this material. VRC successfully manufactured the sample buttons for testing and analysis. [31]

2.3.2   Bio-inspired patterns

The Lotus Leaf pattern is a solution that has already been implemented for dust mitigation due to a phenomenon known as the "Lotus Effect" where the micro and nano papillae cause water to bead up, collect dirt, and slide off [8]. Most applications use a relatively soft medium such as a polymer [4]. The most common method is soft-lithographic duplication. Soft lithography consists of forming a mold of the structure by pouring polydimethylsiloxane (PDMS) onto a piece of the lotus leaf, treating the mold, printing the desired substrate into the mold, and finally removing the mold and treating the new daughter surface [3]. Since the structures are directly copied and not replicated, the super hydrophobicity is better resembled. The creation of a mold allows for the structure to be duplicated reliably, frequently, and with ease. However, due to the methodology required to get the material into the mold, Tungsten-Carbide would be unusable since it is not malleable enough to be pushed into the mold without breaking the mold and its melting point of ~5200°F (2,870 °C) would prevent it from being hardened into the mold due to the PDMS's extremely low melting point of -40°F (-40°C).

On the other hand, the Desert Beetle pattern has been successfully implemented for abrasion resistance in various materials. The pattern features hydrophobic regions, which helps in minimizing wear from abrasive particles [12]. Implementing this pattern onto a ceramic coating like WC-Co is a novel approach that presents significant challenges due to the material's hardness and high melting point. Traditional soft lithography methods, commonly used for softer materials, are not suitable for ceramics like WC-Co because the aforementioned high temperatures required would damage the mold [13].

To address these challenges, advanced manufacturing methods have been explored. Laser surface texturing, a subtractive technique, uses high-powered lasers to ablate the ceramic surface, creating the desired Desert Beetle pattern with precision. This method has been shown to achieve patterning depths of up to 10 micrometers without compromising the material's structural integrity [14]. Additionally, additive manufacturing techniques, such as direct ink writing (DIW), allow for the precise deposition of material to form the intricate microstructures of the Desert Beetle pattern layer by layer, achieving feature sizes as small as 5 micrometers [15]. These methods enable reliable and repeatable application of the pattern to WC-Co coatings, enhancing their abrasive resistance and durability.

2.3.3 Subtractive Approach

For subtractive manufacturing, the Keyence 3-Axis UV Laser Marker was to be used to ablate the patterns into the WC-Co coating. Laser etching isn't a new technology, but it isn't common for use at such low resolutions. In this case, the UV Laser Marker was used at 2W (80% of total power), 100mm/s scan speed, 40kHz pulse frequency, 13 repetitions, and a 0.015mm fill interval on a 1-inch diameter disk of Aluminum-6061. The pattern was a 16x16 grid of 0.1mm diameter holes with a center separation of 0.07mm and a depth of 0.5mm.

It is possible to create a structure at the designated resolution with the UV Laser Marker, however, the device is limited to manufacturing at a low complexity, which led to the Beetle pattern being observed as cylindrical indentations instead of spherical. As seen in Figure 3, the beetle pattern is slightly visible but mostly covered under the leftover debris of Aluminum. This is caused by the marked material from the pattern solidifying and covering the surface of the pattern. The graph shows how the debris clutters the surface from ~400µm and ~800µm on the x-axis. This result would not be usable to prevent dust adhesion since most of the formed pattern is covered in debris. This would be the same result if done on the WC-Co coating. Due to these reasons, the Cold Sprayed coating samples were not ablated for this paper's analysis.

There are still other subtractive manufacturing methods that would work with a material as hard as Tungsten-Carbide. Laser pulse ablation has been proven effective for Tungsten-Carbide at the micro-scale [5]. Ultra Short Pulse Laser (USPL) ablation refers to pulse ablation on the picosecond (ps) and femtosecond (fs) pulse period. The short-duration pulses allow for less material to be removed leading to high accuracy at the micron level. As opposed to the UV Laser Marker, there are high-power USPL ablators that can operate at 300W. This allows for most of the excess material to be vaporized rather than melted onto the surface as observed with the UV Laser Marker.

2.3.4 Additive Approach

Although resin and extrusion-based 3D printing for plastics has existed for over 40 years, ceramics' hardness and temperature resistance have made it very difficult to be used in the same application. The current state of the art additive manufacturing methods for ceramics includes laminated object

manufacturing (LOM), fused deposition modeling (FDM), stereolithography, and digital light processing (DLP). Out of these, the lithography-based methods (stereolithography and digital light processing) yield the best resolution. DLP is a form of indirect AM (additive manufacturing) meaning that it requires an organic binder as well as the ceramic in powder form. This means that the binder would have to be removed before the final product is achieved [7].

Lithography-based ceramic manufacturing (LCM) is an indirect AM method that uses a DLP photopolymerization process developed by Lithoz. The CeraFab S65 printer implemented LCM to make samples of the Lotus Leaf, Beetle, and Control surfaces at a standard 1mm thickness, 12.7mm diameter and two separate surface thicknesses of 25μm and 10μm for the Lotus Leaf and Beetle. Each sample was sintered with a direct sintering method and a debind and sintering method. The direct sintering method is the typical sintering method used to yield the final structure whereas the debind and sinter process does an initial treatment to remove the organic binder and then has the direct sintering done on it. These methods are compared later under the discussion of testing results.

2.4   Verification of the Solution

2.4.1   Mitigating Dust Adhesion

The Tap Tap test is intended to determine the adhesion levels of various surface modifications applied to ceramic. In this case, the Lotus Leaf and Beetle samples have an additional coating thickness of 25 microns. The samples include Control direct, Control debind and sintered; Lotus Leaf direct 1, Lotus Leaf direct 2; Beetle direct 1, Beetle direct 2; Lotus Leaf debind and sintered 1, Lotus Leaf debind and sintered 2; Beetle debind and sintered 1, and Beetle debind and sintered 2. This test began by weighing with a scale of a precision of 0.0001g and imaging the sample with the VHX digital microscope to get a 20x 2D image, 200x 2D image, 200x color profile, and 200x depth profile image. The samples are then placed inside a collection box inside a fume hood with three sieves on top of it to prevent clumping of regolith particles as shown in Figure 20. The mesh sizes used in this experiment are 0.074mm, 0.18mm, and 2mm. The samples are then uniformly covered with ~5g of the chosen regolith simulant, LSP-1D. After the samples are covered in regolith, they are placed vertically and tapped twice to allow excess dust to fall out. Then the sample is weighed and imaged once more.

2.4.2   Impact Analysis – Grit Blaster

The experimental setup for the control sample involved weighing a 1-inch stainless steel sample cold spray coated with WC-Co by VRC Metal Systems and blasting it with 50 grams of LSP-1D lunar simulant using the MicroLux Grit Blaster attached to the Stinger 2.5L wet/dry vacuum's vacuum feature. Afterwards, the surface was brushed off three times, and then the sides and bottom surfaces were dusted off until they were free of visible simulant. The sample was then weighed again using a precision scale, and high-resolution images were taken under the VHX microscope for the 20x 2D image, 200x 2D image, 200x color profile, and 200x depth profile image settings. This process was repeated for three cycles, with the initial weight for each cycle being the final mass of the previous cycle. Due to time constraints, only the control sample without the surface modification was tested and only able to conduct three cycles. The use of 50 grams of lunar simulant per cycle was chosen based on preliminary tests to ensure a consistent abrasive impact, considering the simulant's tendency to clump and disrupt steady mass flow. The lance was inserted into the top port membrane, positioned perpendicular to the sample surface secured with double-sided tape, ensuring

a consistent blast pattern by keeping the other end open for pressure equilibration. This experimental setup is shown in Figure 27.

This setup ensured reliable and repeatable results, including the initial and final masses of the sample for each cycle and high-resolution microscopic images of the surface. The primary objectives were to use a microscope for visual analysis of the coating and a scale to record the sample's mass, determining the abrasive resistance capabilities of the cold sprayed WC-Co coating with Lotus Leaf and Desert Beetle surface modifications. Although only the control sample was tested, the methodology provides a foundation for future experiments with these patterns. The detailed steps and controlled variables facilitate replication and further research, contributing to the development of more durable coatings for lunar landers, enhancing the longevity and performance of critical components in the harsh lunar environment.

2.4.3   Future Testing

The further development and maturation of these bio-inspired surface modifications will require various testing and analysis to validate the effective adhesion resistance. The Taber Abraser test will test the wear resistance of the WC-Co coating and analyze characterizing the wear at a high number of cycles. The Sonic Wand test is an adhesion experiment that is expected to yield more accurate data in determining the amount of lunar dust that adheres to the surface of the coatings. To confirm the temperature ranges of WC-Co found through various research papers these tests will be conducted on our coatings. A chemical exposure test will be conducted to determine the coating resistance to chemical wear after the surface modifications are made to ensure the coating still withstands this type of wear. These tests are planned to be conducted to further gather data to analyze the overall effectiveness and feasibility of the technology being implemented on future HLS missions.

3   Key Finding

3.1   Technological Readiness

The technology used in the creation of the team's proposed solution is largely experimental, each with a varying readiness level. Developing these technologies will be a crucial part of the eventual implementation of the coating in NASA's Artemis program.

Currently, the 3-Axis UV Marker is not at a level where it can make complex microstructures such as the Lotus Leaf and Beetle patterns. On top of this, the maximum power of the laser leads to melted material resolidifying on top of the microstructure making the ablation process inadequate. However, using USPL ablation allows for the process to be run more precisely, with complexities, and at a higher power. As a result, this allows for the material to be vaporized and vacuumed out rather than melted onto the surface. Even with this method, it would require several iterations due to the size constraints of the machinery.

The cold spray application by VRC has been used in various fields including submarine and aircraft maintenance. For this reason, there should be no current limitations to the scale or issues dealing with irregular shapes.

Although Lithoz's LCM can yield high resolution microstructures it suffers in the number of usable materials and scale. Since the 3D printing process uses photocuring, only light powders are usable. Unfortunately, this prevents the WC-Co from being used since it is a dark ceramic powder. However, there may be other AM methods that allow for dark powders to be used. The building envelope of the CeraFab

S65 is 102mm x 64mm x 320mm. Even though it is possible to produce smaller parts, in an iterative development stage, it would take weeks to fully cover the required area, making it extremely inefficient.

3.2   Testing Results and Discussion

3.2.1   Tap Tap Test Results

The Tap Tap test is meant to compare the adhesion levels between the Lotus Leaf pattern, the Beetle pattern, and a control with no surface modifications. This is done by comparing the initial and final masses of each sample after testing to find the amount of regolith mass adhered to the surface. A visual analysis was also done using the VHX digital microscope. A 2D 20x image gives a full comparison of the sample whereas the 2D 200x image, 200x height-color map, and the 200x depth analysis allow for analysis at key points.

The expected result of this experiment was a much lower regolith adhesion for the Lotus Leaf pattern due to its anti-adhesion properties and higher adhesion for the Beetle and Control samples. However, as seen on Table 2, the Beetle patterns ended up performing slightly better than the Control samples and much better than the Lotus Leaf patterns. Using the data from Table 2, the Beetle Pattern achieved an average change in mass of 0.000825g, the Control achieved a change in mass of 0.00155g, and finally the Lotus Leaf pattern achieved a change in mass of 0.010175g. As seen in comparing Figures 14 and 15, the Lotus Leaf pattern allowed for regolith to fall in between the micro pillars and trap it within. Figure 16 shows how the regolith infiltrates the pattern and flattens the distinct peaks of the Lotus Leaf pattern. Although the gap of ~50microns between the pillars is larger than the largest particle size of LSP-1D of 30 microns, the lunar simulant tends to form clumps due to the cohesion of the substance. This issue can be resolved by reducing the distance between the pillars and adding in the nano pillars.

The Beetle and Control samples ended up performing similarly with little resultant adhesion on the surface of the sample seen by comparing the average change in mass. Figures 21 and 22 show specific areas on the two samples where regolith did adhere. Even though the largest possible particles size of the simulant is only 30 microns, the peaks found from the adhered regolith resemble differences of over 100 microns. This is caused by the LSP-1D's cohesion resulting in clumps forming like what was seen on the Lotus Leaf pattern.

Although this test can show the basic adhesion of LSP-1D onto different surface patterns, the test is very crude and not representative of an actual scenario under which adhesion would occur. A more comprehensive adhesion will need to be done to gather more conclusive results as to which pattern has the lowest adhesion.

After comparing the corresponding samples direct sintered and debind sintered initial masses from Table 2, it is observed that there was almost no mass difference between the two sintering methods. To speed up sample production at a larger scale, it would be beneficial to only do the direct sintering method instead of doing the debinding process.

3.2.2   Grit Blaster Test Results

The grit blaster test is designed to test the abrasive effects of lunar regolith on various surface coatings. By subjecting samples coated with cold-sprayed WC-Co to a controlled stream of lunar simulant, the durability and resistance of the coating under conditions like those encountered during lunar landings was assessed.

Specifically, this test is crucial for determining the effectiveness of the coatings and the surface modifications in protecting the structural integrity of the HLS.

To quantify the results using mass, each sample was weighed before and after being subjected to the grit blasting process, with the initial weight for each cycle taken as the final mass from the previous cycle. As shown in Figure 17, the sample experienced a mass increase of 0.0024 g in Cycle 1, a mass loss of 0.0006 g in Cycle 2, and no significant mass change in Cycle 3. These results suggest that the initial cycles involve some material redistribution rather than pure loss, possibly due to abraded particles reattaching to the surface. The significant impact of abrasion on the coated surface is evident in the mass loss in Cycle 2. The recirculation of simulant particles within the vacuum chamber likely contributed to abrasion on the sides and non-coated areas. In vacuum conditions, minimal air resistance allows particles to travel freely and at high velocities, leading to increased mobility and dispersion [16]. This effect is akin to plume-surface interactions on lunar landers, where high-speed ejecta causes erosion on various surfaces [17]. The consistent mass loss indicates the enhanced abrasive resistance of the HLS and ensures the durability of critical components during lunar missions.

On the other hand, to qualitatively assess the surface, high-resolution images of each sample were taken using a VHX microscope at 200x magnification before and after grit blasting, across all three cycles. The images included 2D, depth composition, and height color map views, providing a comprehensive visualization of surface changes. As shown in Figures 7 & 24, for Cycle 1, the depth composition and color map images revealed significant surface roughness and initial signs of wear, with depth variations up to 56.85 microns. In Figures 8 & 25, for Cycle 2, the depth composition and color map images showed increased surface irregularities and deeper pits, with depth variations up to 31.26 microns. In Figures 9 & 26, for Cycle 3, the depth composition and color map images indicated stabilized degradation with minimal additional wear, showing depth variation up to 128.94 microns. In Figure 23, pre-grit blast images displayed a relatively smooth surface, with post-blast images revealing significant material removal and surface pitting. These qualitative observations partially align with the quantitative mass data, suggesting that while the mass data shows minimal changes, the surface still experiences significant roughening and degradation, confirming the abrasive impact of the lunar simulant and the need for enhanced coating durability in the HLS.

To quantify the results using color intensity, high-resolution 200x, 2D images from each cycle were analyzed by converting them to grayscale and performing histogram analysis using MATLAB to understand the distribution of pixel intensities. As shown in Figure 10, the mean intensity and standard deviation were calculated for each cycle: Cycle 1 had a mean intensity of 125.84 and a standard deviation of 22.12, Cycle 2 had a mean intensity of 126.49 and a standard deviation of 18.84, and Cycle 3 had a mean intensity of 125.63 and a standard deviation of 22.36.

The mean intensity represents the average brightness of the surface, indicating the overall level of abrasion. The standard deviation measures the variation in brightness, which correlates with the surface roughness and irregularities. The slight variation in mean intensity across cycles suggests that the overall brightness of the surface remains relatively consistent. However, the changes in standard deviation indicate differences in surface texture and roughness.

In Cycle 1, the standard deviation of 22.12 indicates some initial surface irregularities due to the abrasive action. In Cycle 2, the decrease in standard deviation to 18.84 suggests a temporary smoothing effect,

possibly due to the redistribution of abraded particles. By Cycle 3, the standard deviation increases again to 22.36, reflecting increased surface irregularities and roughness due to continued abrasive action.

The changes in color intensity directly correlate with the mass data and the visual surface degradation observed in the other analyses. Specifically, the mean intensity values provide an indication of the overall surface condition, while the standard deviation reflects the degree of surface roughness and irregularities. In the initial cycle, the significant mass gain corresponds to a higher standard deviation, indicating increased surface roughness due to abrasive action. As the mass loss stabilizes in Cycle 3, the mean intensity remains relatively constant, but the standard deviation increases again, suggesting that while the material loss has plateaued, the surface continues to experience fine-scale roughening and degradation. This correlation between the quantitative color intensity measures and the mass loss data underscores the progressive nature of the abrasive damage and the limitations of the current WC-Co coating without additional surface modifications.

3.3   Programmatic Implementation

Ceramics coatings offer a diverse array of applications for human landers. These investigations into both additive and subtractive approaches have demonstrated the ability for these coatings to be readably implemented to human lander missions. Working with our corporate partners, the original understanding and application of ceramic coatings has been broadened to include new possibilities which are important to highlight. Our initial approaches consist of the application of Tungsten Carbide through Cold Spray, and 3D printing alumina ceramic tiles with biomimetic patterns. Cold Spray technology has shown the ability to enhance the wear and corrosion resistance of a given surface and can service larger vehicles. VRC Metal systems has recently partnered with the U.S. Navy to service and repair its fleet of submarines in California, demonstrating Cold Sprays capabilities for integration into larger vehicles and products. Working with Lithoz to develop our 3D printed ceramic tiles, we successfully were able to develop our biomimetic patterns using Alumina. As a result, new considerations have been made to develop and test transparent ceramic tiles with a similar pattern for the application to windows, sensors, and lenses. This potential capability has been demonstrated before by Alfred University and is a current Lithoz capability.

The application of ceramics goes beyond that of providing structural integrity for spacecraft. Ceramics were used on previous spacecraft and are still explored as innovative solutions to thermal control. The Japan Aerospace Exploration Agency (JAXA) has previously developed and tested "smart radiation devices" which have a variable emissivity based on temperature. These thin ceramic tiles are based on Lanthanum Strontium Manganite Oxides (LSMO) which can be further enhanced using MLI's to reduce solar absorptivity. This technology has been tested on the Reimei satellite and Hayabusa asteroid explorer highlighting the potential use of thin ceramic tiles in thermal regulation for spacecraft.

Another critical area where the current design implementation of WC-Co would not be applicable is the windows of the HLS. Since the main goal is to allow light to pass through, an opaque ceramic coating such as WC-Co would not be viable. An alternative approach would be to use a transparent ceramic coating. Currently, the main options for this are Alumina (Al_2O_3) and Zirconia (ZrO_2). The key to the manufacturing of this special ceramic is using nanocrystalline (mean grain size <100nm) Alumina powder alongside consolidated with SPS (Spark Plasma Sintering) and (HP) Hot Pressing [1]. To achieve true transparency, the mean grain size of the powder must be less than the incident wavelength of light [2]. Unfortunately, when adding a surface modification such as the Lotus Leaf pattern or the Beetle pattern, there are light

dispersion effects that prevent a clear image through the window. Testing needs to be done to better understand and analyze how surface finishes affect visibility.

3.4   Risk Matrix Analysis

When assessing the various risks associated with our proposed coating, it can be determined that the benefits of the application of a ceramic coating to the human lander outweigh the potential drawbacks. Our team developed a risk matrix to evaluate various risks that could befall the human lander from the application of our coating. The potential risk and risk matrix can be viewed in the Appendix below. From investigating further into the indicated risks, the only risk that can pose a significant impact on the human lander would be thermal mismatch. The chosen human landers for the Artemis missions are assumed to be mostly comprised of Al-6061, or 300 type stainless steels. When considering the thermal expansion coefficients of these materials in reference to Tungsten Carbide, the discrepancy between these values creates thermal stresses. These thermal stresses can compromise the integrity of the human lander or WC coating by warping, or cracking at points where these materials are in contact. There are various solutions to minimize these negative effects, each of which would require further testing. Some of the prominent strategies that could be implemented to the human lander and our coating would be introducing an intermediate layer or investigating other thermal protection systems.

4   Realistic Assessment of Costs

As seen in Table 1, using the dimensions of the Apollo Lunar Module as a proxy for the HLS, cost calculations were performed based on the dimensions and prices of coated samples that were used for the grit blaster experiment provided by VRC Metal Systems. Specifically, VRC coated 21 samples with a 1-inch diameter and a thickness of 0.010 inches. This geometric estimation was scaled up to match the dimensions of the lunar lander legs [32], assuming the leg struts are cylindrical, which is consistent with the Apollo Lunar Module design [33] [34]. The windows, however, for the ascent stage were used to asset the cost of coating. Using the methodology of the lander legs this was used for the window. The windows on the ascent stage of apollo were two 25-inch by 28-inch triangle size [36]. For the assumption of cost calculation and assumption of five windows using the dimensions of the ascent stage apollo 11 windows. Additional costs beyond the coating process include operational expenses to maintain the coating's integrity during the mission, covering labor and logistical costs. However, since the coating provides a passive solution for lunar dust mitigation, these costs are limited to the initial application and related activities during mission development. The Apollo Lunar Module's dimensions were used because they are well-documented, and the Artemis HLS is still in developmental process, with exact dimensions not yet finalized, making the former a reliable reference for preliminary costs estimations [35]. The Apollo Lunar Module serves as a valuable reference due to its successful design and operation in similar lunar conditions, which can provide insights into the requirements and challenges for the Artemis missions. [Table 1]

5   Full Concept Timeline

This project aims to develop a passive mitigation method, characterized by a WC-Co coating using bio-inspired patterns to hinder dust adhesion and abrasion on lunar landers. The first step in this project is initial planning, which involves conducting the initial literature review and defining the budget and objectives from January to March. The literature review would include research on the cold spray deposition method, bio-inspired surface modifications, laser ablation, and microscopic additive manufacturing, to gain a better understanding of up-to-date advancements in these fields. The second step is developing the coatings and

connecting with manufacturing companies from April to December. While this happens, Preliminary testing will occur from October to December, involving the basic adhesion and abrasion testing of initial designs. Leading into the next year, iterative testing will take place as well as refining the coating through detailed tests and adjustments throughout the whole year. Enhanced coating development will occur from May to August, during which additional modifications will be made based on the results. The third year will be the project's last stage, with the coating being finalized and validated between January and June. The project concludes with implementation and deployment from July to December, with production, application of the coating to lunar landers, and post-deployment results. The project timeline chart can be viewed in table 5 section 6.1. A project timeline is crucial to effectively manage time in each phase, from initial planning to final implementation, and ensure that every part is completed on time and within budget. Additionally, it helps track tasks within team members and coordination with manufacturers guaranteeing that the development of the coating stays on track and meets objectives.

6   Appendices

All figures created by the C. R. A. T. E. R. team unless otherwise stated in caption

6.1 Figures and Tables
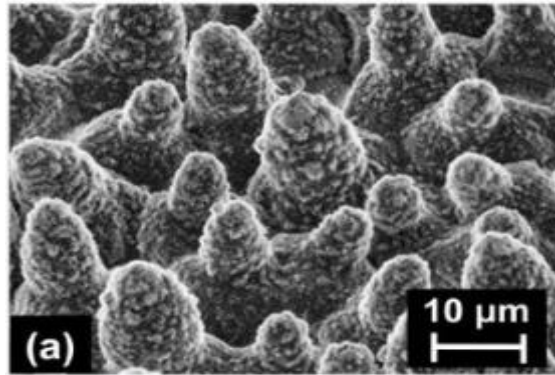
Figure 1: Scanning Electron Microscopy (SEM) of a Lotus Leaf Microstructure [6]
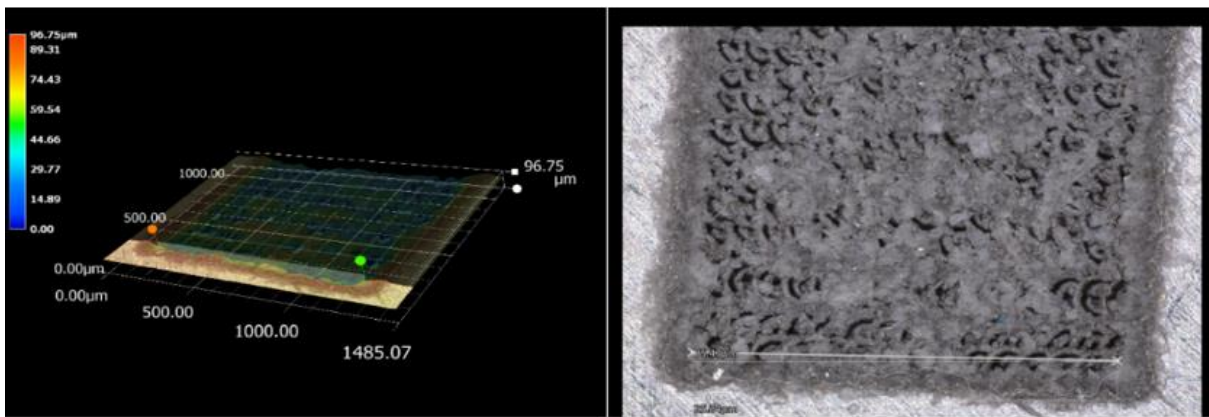
Figure 2: 200x Zoom Imaging of 3D Profile and 2D Image of UV Laser Marker Ablated Desert Beetle Pattern Button Sample
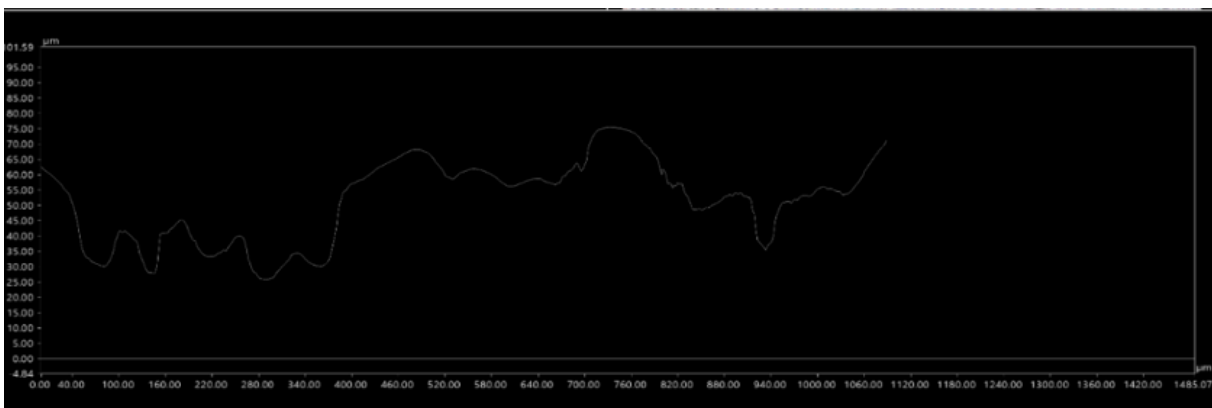
Figure 3: Depth Graph of the Surface of a UV Laser Marker Ablated Desert Beetle Patten Button Sample
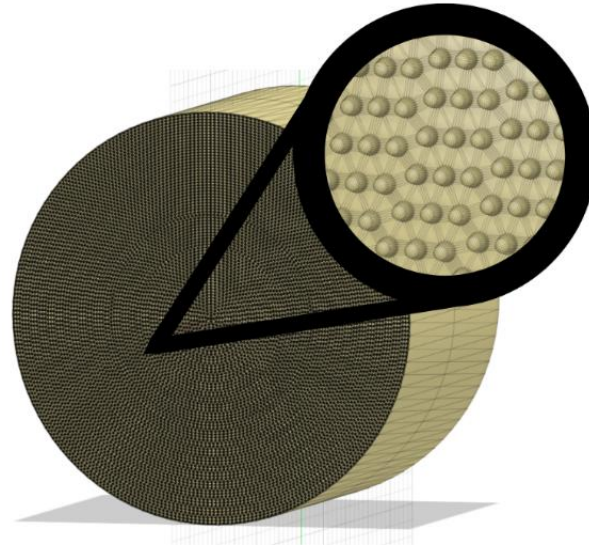
Figure 4: STL File Depiction of Lotus Leaf
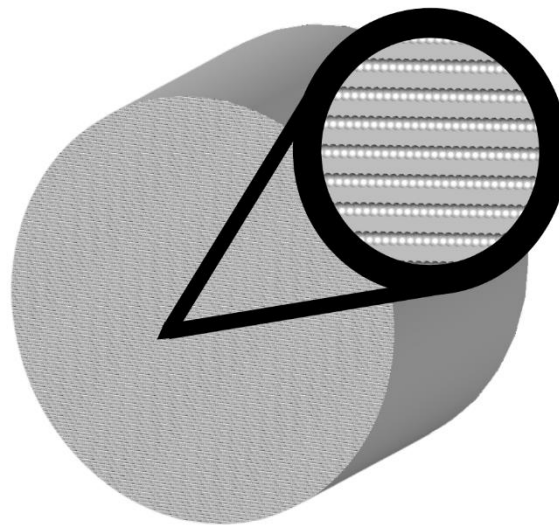
Figure 5: STL File Depiction of the Beetle Pattern

Table 1: Project Cost Estimation

Description	Value
Target Thickness	0.010 in
Surface Area of One Sample	0.7854 in
Cost per Square Inch	$ 265.27 per in
Area of Window	350 in^2
Surface Area of Primary Strut	916.3 in
Total Surface Area of Secondary Struts	9076.2 in
Total Surface Area of Legs	9992.5 in
Estimate Total Cost	$11,051,314.4
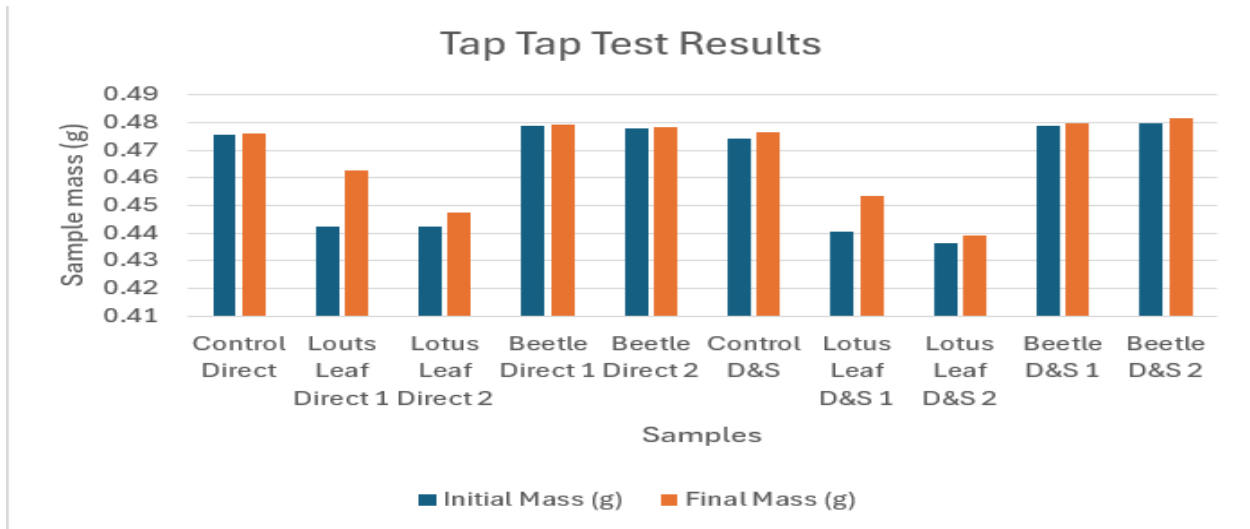
Figure 6: Measurements of Mass Data of the Initial and Final Mass of the Ceramic Tile Sample

	Control Direct	Louts Leaf Direct 1	Lotus Leaf Direct 2	Beetle Direct 1	Beetle Direct 2	Control D&S	Lotus Leaf D&S 1	Lotus Leaf D&S 2	Beetle D&S 1	Beetle D&S 2
Initial Mass (g)	0.4755	0.4426	0.4426	0.4788	0.4781	0.4743	0.4404	0.4365	0.479	0.4797
Final Mass (g)	0.4762	0.4629	0.4474	0.4792	0.4783	0.4767	0.4535	0.439	0.4797	0.4817
Mass Regolith Used (g)	5.016	5.0789	5.01423	5.0806	5.0182	4.9883	5.0204	5.0814	5.0467	5.0814
Change in Mass (g)	0.0007	0.0203	0.0048	0.0004	0.0002	0.0024	0.0131	0.0025	0.0007	0.002

Table 2: Testing Data from the Tap Tap Test Performed on the Ceramic Tile Samples
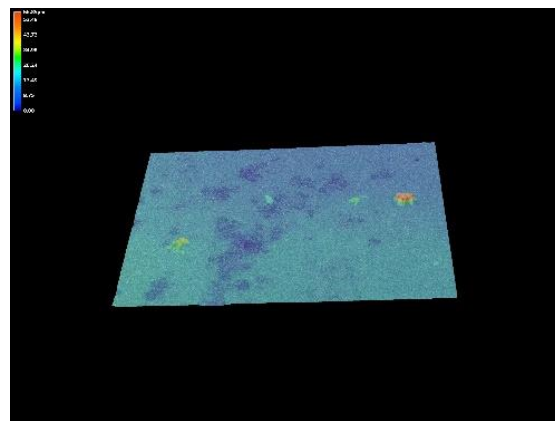
Figure 7: 200x Zoom Color Profile Images of Control Sample Post-Testing for Cycle 1
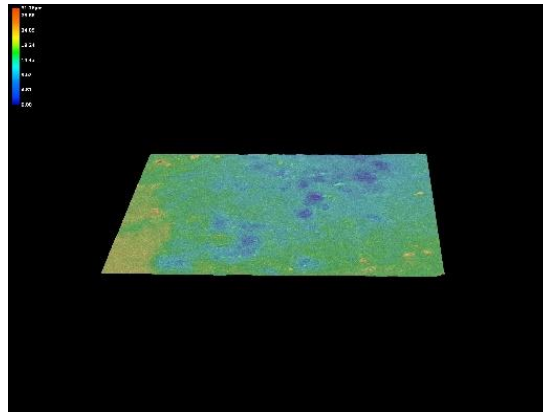
Figure 8: 200x Zoom Color Profile Images of Control Sample Post-Testing for Cycle 2
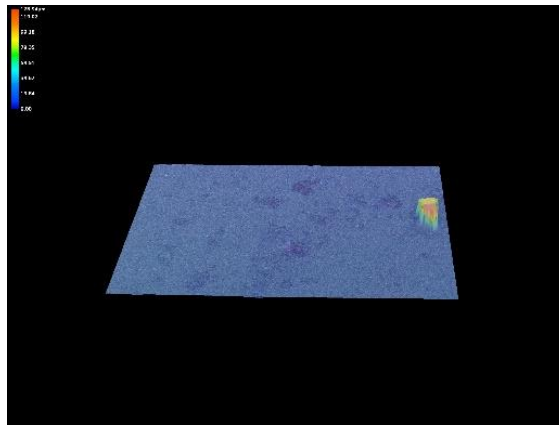
Figure 9: 200x Zoom Color Profile Images of Control Sample Post-Testing for Cycle 3
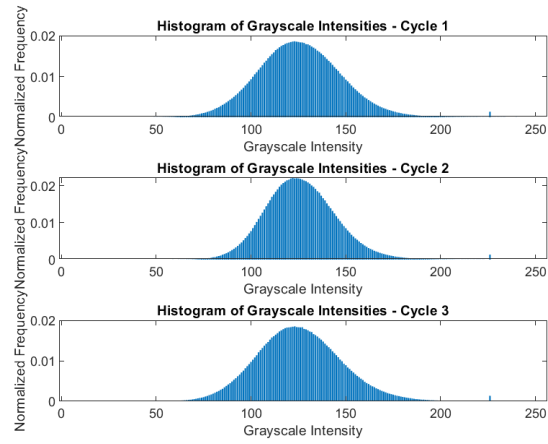
Figure 10: Histogram of the Grayscale Intensities of 200x 2D Images of Each Cycle
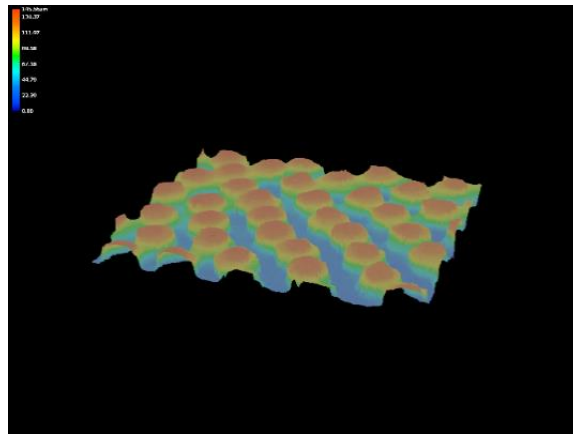
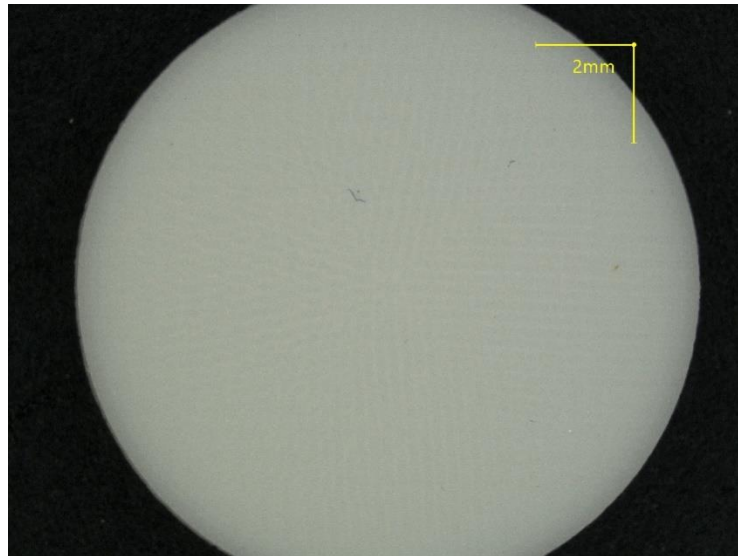*Figure 11:200x Zoom Depth Analysis of Lotus Leaf Pattern Before Testing*
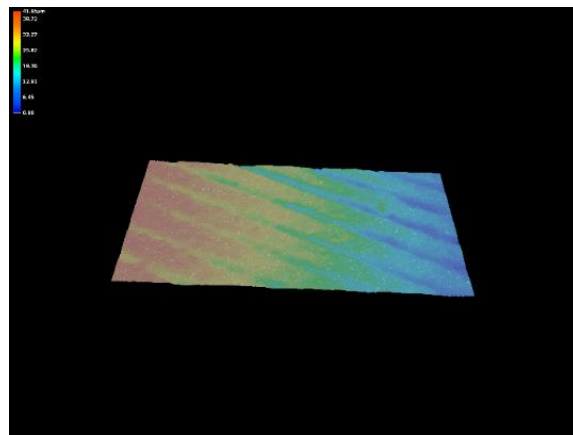
Figure 12: 200x Zoom Depth Analysis of Beetle Pattern Before Testing
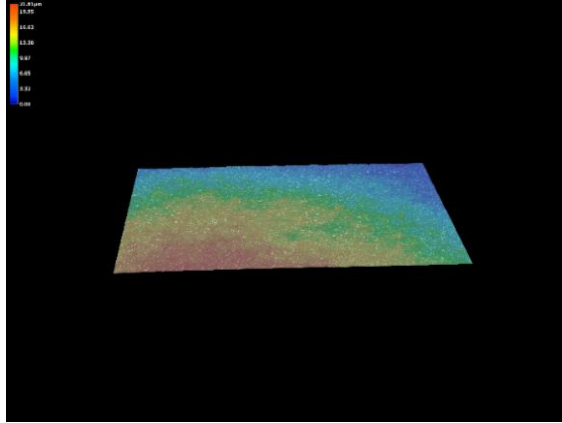
Figure 13: 200x Zoom Depth Analysis of Control Sample Before Testing

Figure 14: 20x Zoom 2D Image of Lotus Leaf Sample before Tap Tap test
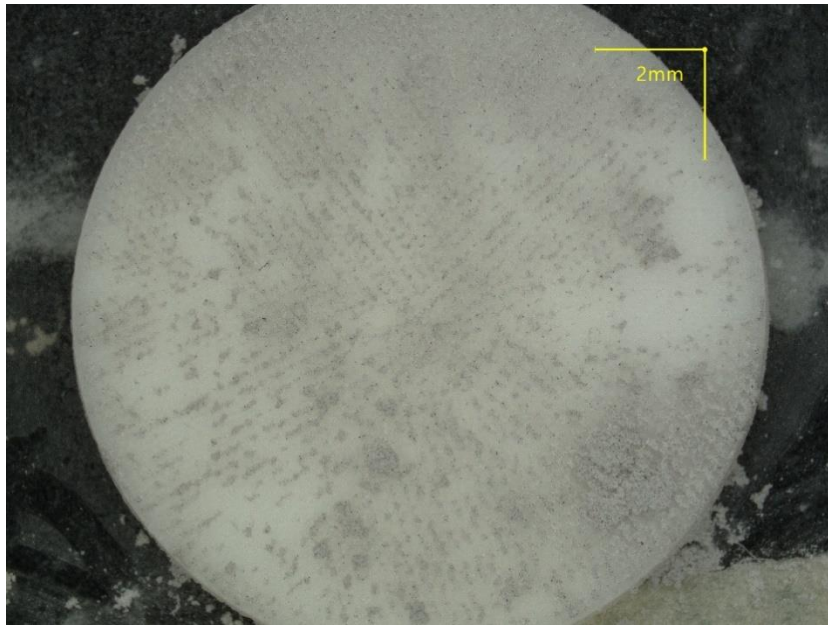
Figure 15: 20x Zoom 2D Image of Lotus Leaf Pattern After Tap Tap Test
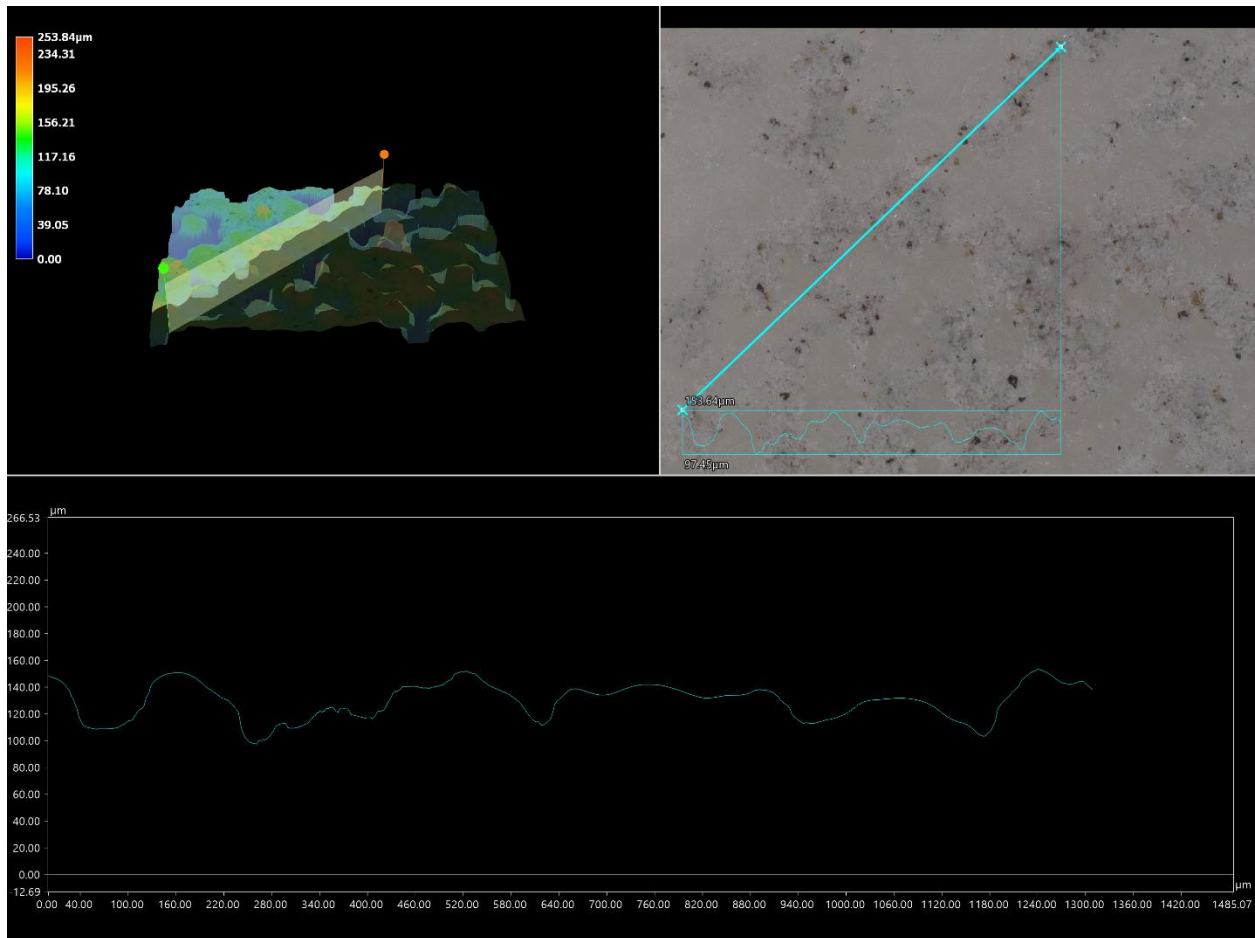
Figure 16: 200x Zoom Depth Analysis Including Height-Color Map of Lotus Leaf Sample after Tap Tap test
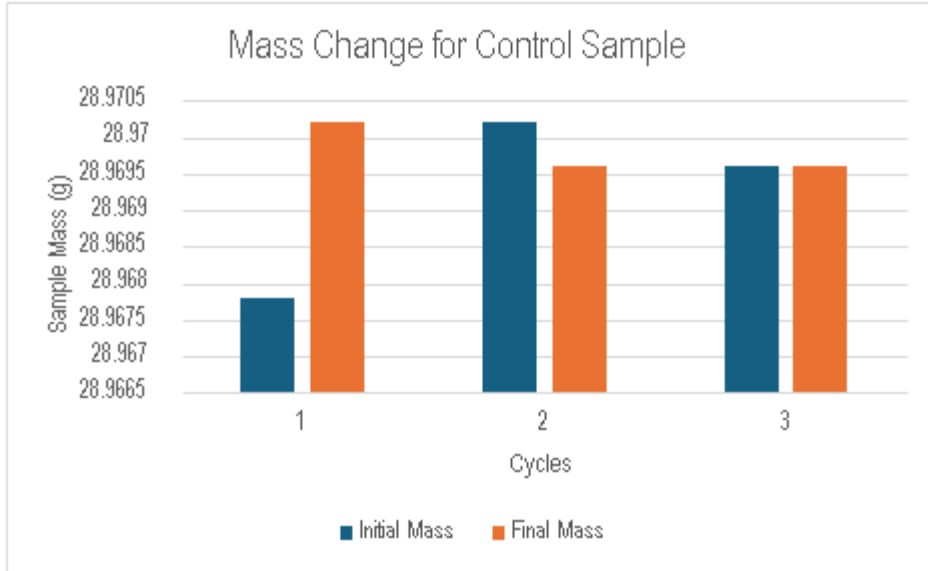
Figure 17: Measurements of Mass Data for Initial and Final Mass of the Control Sample

Table 3: Passive Method for Mitigating Effects of Lunar Regolith

Method	*Surface Coatings*	Brushes and Seals	Self Cleaning Surfaces	Electrodynamic Dust Shield	Lunar Landing Pads
Criteria	Ratings				
Surface Adhesion Resistance	Medium-High	Medium	High	Low-Medium	High
Impact Resistance	Medium	Low-Medium	Medium	Low	High
Abraision Resistance	Medium-High	Medium-High	Medium	Low	High
Ease of Manufacturing	High	Medium	Medium	Medium-High	Medium-High
Cost	Medium	Medium	Medium-High	Low	Medium-High
Complexity	Medium	Low-Medium	Medium-High	High	Medium
Effectiveness	Medium	Medium	Medium-High	High	High
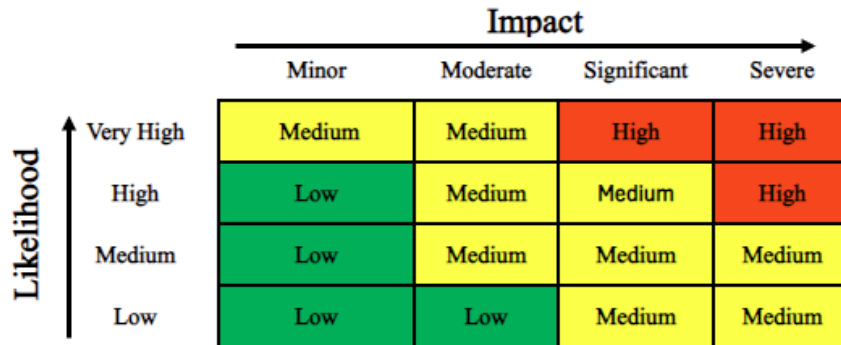
Figure 18: Risk Management Matrix Utilized to Sort Possible Risks for Proposed Solution

Table 4: Risk Matrix Assessment

Name of Risk	Likelihood	Impact
Thermal Mismatch	High	Severe
Micrometeoroid/Debris Impact	Very High	Moderate
Chemical Degradation	Low	Moderate
Mechanical Stress	Low - Medium	Low-Moderate
Manufacturing Defects	Medium	Moderate
Adhesion Failure	Medium	Moderate
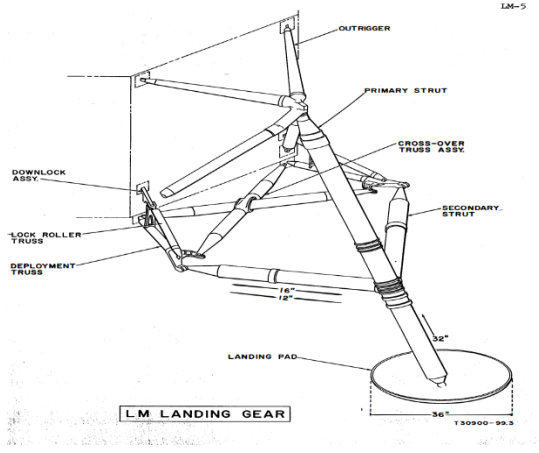
Figure 19: Apollo Lunar Module Landing Gear Diagram with Dimensions [10].

Table 5: Project Time

Dates	Year 1	Year 2	Year 3
Initial Planning and Setup			
Coating Development			
Prototype Development			
Preliminary Testing			
Iterative Testing and Optimization			
Enhanced Coating Development			
Final Optimization and Validation			
Final Coating Development			
Comprehensive Testing			
Implementation and Deployment			

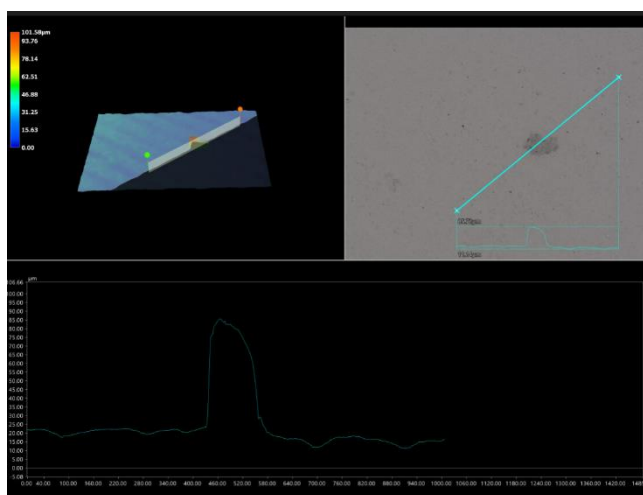*Figure 20: Tap Tap Test Setup*

Figure 11:200x Zoom Depth Analysis including Height-Color Map of Beetle Sample after Tap Tap Test
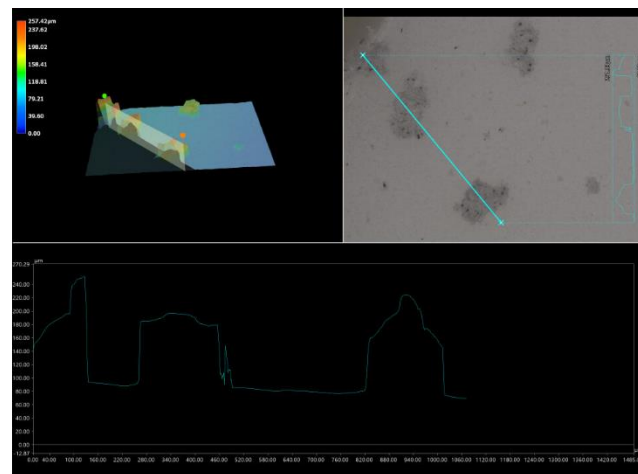

Figure 22:200x Zoom Depth Analysis including Height-Color Map of Control Sample after Tap Tap Test
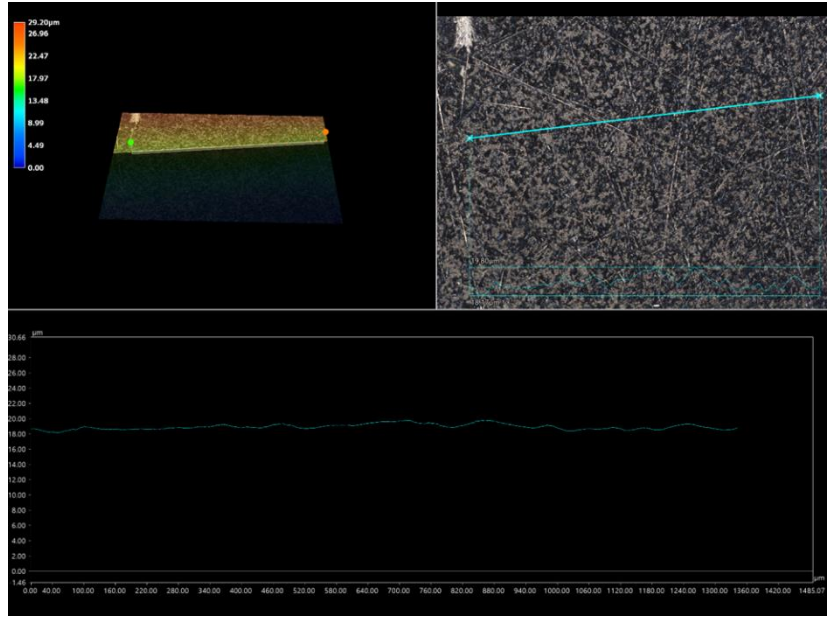
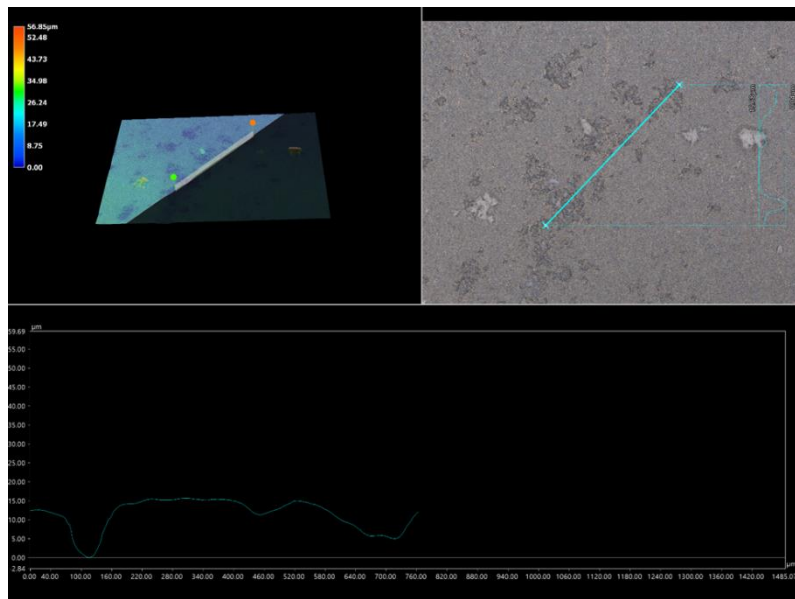*Figure 23: 200x Zoom Depth Composition of Control Sample Pre-Blasting*

Figure 24: 200x Zoom Depth Composition of Control Sample Post- Blasting for Cycle 1
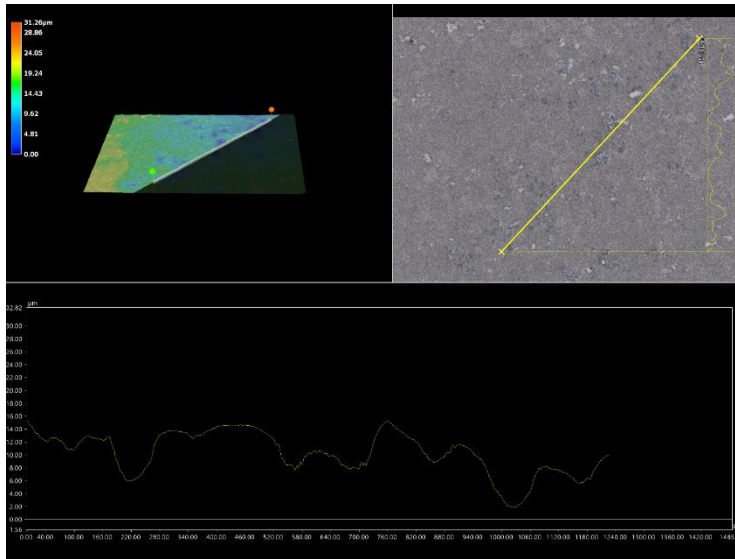
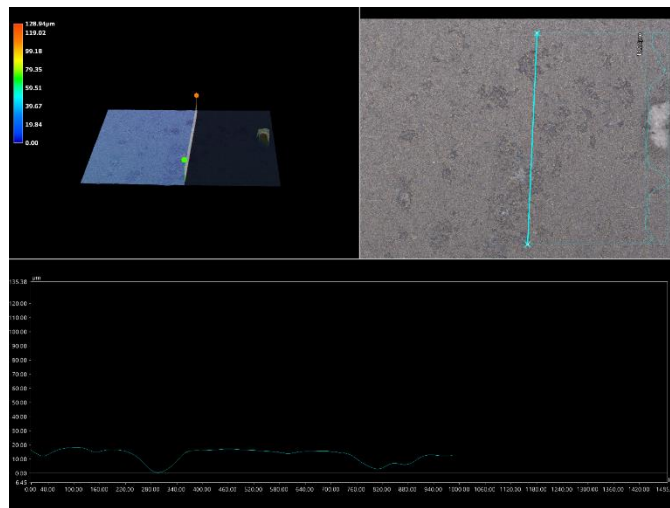*Figure 25: 200x Zoom Depth Composition of Control Sample Post-Blasting for Cycle 2*

Figure 262:200x Zoom Depth Composition of Control Sample Post-Blasting for Cycle 3

Figure 27: Grit Blaster Experiment Setup

6.1   References

[1] Ghanizadeh, S., Grasso, S., Ramanujam, P., Vaidhyanathan, B., Binner, J., Brown, P., Goldwasser J., Improved transparency and hardness in α-alumina ceramics fabricated by high-pressure SPS of nanopowders, Ceramics International, Volume 43, Issue 1, Part A, 2017, Pages 275-281, ISSN 0272-8842

[2] Sokol, M., Kalabukhov, S., Dariel, M. P., Frage, N., High-pressure spark plasma sintering (SPS) of transparent polycrystalline magnesium aluminate spinel (PMAS),Journal of the European Ceramic Society,Volume 34,Issue 16,2014,Pages 4305-4310,ISSN 0955-2219

[3] Yun, X., Xiong, Z., He, Y., & Wang, X., (2020).Superhydrophobic lotus-leaf-like surface made from reduced graphene oxide through soft-lithographic duplication. RSC advances,10(9),5478–5486.

[4] Wood, J., Superhydrophobic polymers cast from lotus leaves: Fabrication & processing, Materials Today, Volume 8, Issue 10, 2005, Page 15, ISSN 1369-7021

[5] Fang, S., Hsu, C-J., Klein, S., Llanes, L., Bähre, D., Mücklich, F., Influence of Laser Pulse Number on the Ablation of Cemented Tungsten Carbides (WC-CoNi) with Different Grain Size.Lubricants.2018; 6(1):11.

[6] Costa, M. N., Veigas, B., Jacob, J. M., Santos, D. S., Gomes, J., Baptista, P. V., Martins, R., Inácio, J., & Fortunato, E. (2014). A low cost, safe, disposable, rapid and self-sustainable paper-based platform for diagnostic testing: Lab-on-paper. Nanotechnology, 25(9), Article 094006. https://doi.org/10.1088/0957-4484/25/9/094006

[7] Schwentenwein, Martin & Homa, Johannes. (2014). Additive Manufacturing of Dense Alumina Ceramics. International Journal of Applied Ceramic Technology.12.10.1111/ijac.12319.

[8] Latthe, S.S., Terashima, C., Nakata, K., & Fujishima, A. (2014). Superhydrophobic surfaces developed by mimicking hierarchical surface morphology of lotus leaf. Molecules (Basel, Switzerland),19(4),4256–4283.

[9] NASA. (1969). *Apollo 11 Lunar Module / EASEP*. NASA Space Science Data Coordinated Archive. Retrieved from https://nssdc.gsfc.nasa.gov/nmc/spacecraft/display.action?id=1969-059C

[10] Bryan, C., Strasburger, W., & Kalkowsky, H. (1969). Lunar Module Structures Handout LM-5. *NASA, May*. https://www.nasa.gov/wp-content/uploads/static/history/alsj/a11/a11LM5structures.pdf

[11] Tillmann, W., Hagen, L., Stangier, D., Laemmerhirt, I.-A., Biermann, D., Kersting, P., & Krebs, E. (2015). Wear behavior of bio-inspired and technologically structured HVOF sprayed NiCrBSiFe coatings. *Surface & Coatings Technology*, *280*, 16–26. https://doi.org/10.1016/j.surfcoat.2015.08.055

[12] Parker, A. R., & Lawrence, C. R. (2001). Water Capture by a Desert Beetle. *Nature*, 414(6859), 33-34.

[13] Beckett, A., & Ginley, D. (2016). Surface Texturing Inspired by the Namib Desert Beetle. *Journal of Materials Science*, 51(2), 432-443.

[14] Lee, C., Kim, C., & Byun, D. (2014). Effects of Hydrophilic-Hydrophobic Patterns on Dust Removal. *Applied Surface Science*, 290, 458-463.

[15] Watson, G. S., Cribb, B. W., & Watson, J. A. (2010). Experimental Determination of the Efficiency of Water Collection on Biomimetic Analogs of a Moth's Eye and the Namib Desert Beetle. *Langmuir*, 26(24), 15976-15981.

[16] Smith, J., & Johnson, R. (2017). Particle dynamics in vacuum conditions: Implications for material erosion. *Journal of Applied Physics*, 120(12), 12345.

[17] Metzger, P. T., Lane, J. E., & Immer, C. D. (2011). Rocket blast erosion effects lunar soil. *Earth and Space Conference 2010*, 114-123.

[18] Tachikawa, S., Nagano, H., Ohnishi, A. et al. Advanced Passive Thermal Control Materials and Devices for Spacecraft: A Review. Int J Thermophys 43, 91 (2022). https://doi.org/10.1007/s10765-022-03010-3

[19] Space Environment Exposure Effects on Ceramic Coating for Thermal Protection Systems Roberto Pastore, Andrea Delfini, Fabio Santoni, Mario Marchetti, Marta Albano, Fabrizio Piergentili, and Roberto Matassa Journal of Spacecraft and Rockets 2021 58:5,1387-1393 https://doi.org/10.2514/1.A34997

[20] MatWeb, *Overview of Materials for T 300 Series Stainless Steel (*n.d.). https://www.matweb.com/search/DataSheet.aspx?MatGUID=7a87941825a3463eaba7979c4333721f

[20] Aerospace Specification Metal Inc, *Aluminum 6061-T6; 6061-T651 Material Data Sheet*. (n.d.). https://asm.matweb.com/search/specificmaterial.asp?bassnum=ma6061t6

[21] AZoM, *Properties: Tungsten Carbide - an overview*. (n.d.). https://www.azom.com/properties.aspx?ArticleID=1203

[22] Osthus, R. (2023, September 15). *U.S. Navy partners with VRC metal systems: VRC Metal Systems: Box elder, SD*. VRC Metal Systems. https://vrcmetalsystems.com/u-s-navy-partners-with-vrc-metal-systems-for-fleet-repair/

[23] Zhang, G., & Wu, Y. (2021). Three-dimensional printing of transparent ceramics by lithography-based digital projection. *Additive Manufacturing*, *47*, 102271. https://doi.org/10.1016/j.addma.2021.102271

[24] Thermal control of a light-weight rover system in the ... (n.d.). https://ttu-ir.tdl.org/server/api/core/bitstreams/cb1fc91f-ba1e-44a4-970a-08d54c6ef7bc/content

[25] Verstak, A. (2017, August 28). *Kermetico*. Tungsten carbide coating properties HVAF thermal spraying WC-10Co-4C. https://kermetico.com/coating-materials/wccocr-hvaf-tungsten-carbide-coatings-properties-structure

[26] Rao, N. S., & Griffin, B. N. (1993). Effective Planetary Exploration, Part 1: A Heuristic Method to Estimate EVA Walkback Range. *SAE Transactions*, *102*, 1390–1399. http://www.jstor.org/stable/44740086

[27] Harald Hiesinger, Ralf Jaumann, Chapter 23 - The Moon, Editor(s): Tilman Spohn, Doris Breuer, Torrence V. Johnson, Encyclopedia of the Solar System (Third Edition), Elsevier, 2014, Pages 493-538, ISBN 9780124158450, https://doi.org/10.1016/B978-0-12-415845-0.00023-2.

[28] Z. Geng, S. Li, D.L. Duan, Y. Liu, Wear behavior of WC–Co HVOF coatings at different temperatures in air and argon, Wear, Volumes 330–331, 2015, Pages 348-353, ISSN 0043-1648, https://doi.org/10.1016/j.wear.2015.01.035.

[29] Reitz, G., Berger, T., Matthiae, D., Radiation exposure in the moon environment, Planetary and Space Science, Volume 74, Issue 1, 2012, Pages 78-83, ISSN 0032-0633, https://doi.org/10.1016/j.pss.2012.07.014.

[30] NASA. (n.d.). *Moon fact sheet*. NASA. https://nssdc.gsfc.nasa.gov/planetary/factsheet/moonfact.html

[31] Osthus, R. (2021, April 20). *What is cold spray: VRC Metal Systems: Box elder, SD*. VRC Metal Systems. https://vrcmetalsystems.com/what-is-cold-spray/

[32] Apollo Lunar Module Structures. Retrieved from https://www.nasa.gov/wp-content/uploads/static/history/alsj/a11/a11LM5structures.pdf

[33] NASA. (1972). Apollo experience report: Lunar module landing gear subsystem. Retrieved from https://ntrs.nasa.gov/archive/nasa/casi.ntrs.nasa.gov/19720018253.pdf

[34] Rogers, W.F. (1973). Apollo Lunar Module Landing Gear. Retrieved from https://ntrs.nasa.gov/api/citations/19730010151/downloads/19730010151.pdf

[35] NASA. (2024). Human Landing System (HLS) Overview. Retrieved from https://ntrs.nasa.gov/api/citations/20220013431/downloads/HLS%20IAC_Final.pdf

[36] Spacecraft Structural Windows. (n.d.-a). https://www.lpi.usra.edu/lunar/documents/apolloSpacecraftWindows.pdf

6.2   Calculations

6.2.1   Calculation Correction of Mass Change

m = ρV = ρlA = (14.9 g/cm^3)(0.025 cm)(1 cm^2) = 0.3725 g

m = ρV = ρlA = (14.9 g/cm^3)(0.025 cm)(1 cm^2) = 0.37846 g

6.2.2 Calculations of Estimated Cost

Geometric Calculation:

- Sample Calculation

  Diameter: 1 inch
  Target thickness: 0.010 inch
  Surface Area of One Sample = $\pi r^2 = \pi (0.5)^2 = 0.7854$ in^2

- Legs Calculation

Primary Strut
Diameter: 4.5 inches
Length: 64 inches
Surface Area of Cylinder = $2\pi rh + 2\pi r^2 = (2\pi)(2.25)(64) + (2\pi)(2.25)^2 = 916.3$ in^2

Secondary Strut (14 pieces)
Diameter: 3.5 inches
Length: 58 inches
Surface Area of One Secondary Strut = $2\pi rh + 2\pi r^2 = (2\pi)(1.75)(58) + (2\pi)(1.75)^2 = 648.3$ in^2
Total Surface Area of Secondary Struts = $(14)(648.3) = 9076.2$ in^2

Total Surface Area of Legs
Total Surface = Surface Area of Primary Strut + Total Surface Area of Secondary Struts = 916.3 + 9076.2 = 9992.5 in^2

Cost Estimation:

– Using the cost from the sample quote, the cost per square inch for the coating process was estimated. Per Square Inch Cost (assuming the coating will have the desired thickness of 0.010 inch)

Net Unit Price = \$4,375.00 / 21 = \$ 208.34
Surface Area of one sample = 0.7854 in^2
Cost Per Square Inch = Net Unit Price / Surface Area of One Sample = (\$ 208.34)/(0.7854 in^2) = \$ 265.27

– Legs Cost (All four legs)

Total Leg Surface Area = 9992.5 in^2
Cost Per Square Inch = \$ 265.27
Window total area = (350)(5) = 1750 in^2
Window cost = (1750 in^2)(\$ 265.27 per in^2) = \$ 464,222.50
Legs Cost = (4)(Total Leg Surface Area)(Cost Per Square Inch) = (4)(9992.5 in^2)(\$ 265.27 per in^2) = \$10,602,841.90

Total Estimated Cost for Lander Leg and Window Application = \$ 11,067,064.40

6.3 MATLAB Code

Note: Must have Image Processing Toolbox

```
% Load images for each cycle
img_cycle1_2D = imread('SAMPLE3_CYCLE1_2D(200X).tif');
img_cycle2_2D = imread('SAMPLE3_CYCLE2_2D(200X).tif');
img_cycle3_2D = imread('SAMPLE3_CYCLE3_2D(200X).tif');
```

```matlab
% Convert images to grayscale for intensity analysis
gray_cycle1 = rgb2gray(img_cycle1_2D);
gray_cycle2 = rgb2gray(img_cycle2_2D);
gray_cycle3 = rgb2gray(img_cycle3_2D);
% Calculate histogram of grayscale intensities
[counts1, binLocations1] = imhist(gray_cycle1);
[counts2, binLocations2] = imhist(gray_cycle2);
[counts3, binLocations3] = imhist(gray_cycle3);
% Normalize histograms
counts1 = counts1 / sum(counts1);
counts2 = counts2 / sum(counts2);
counts3 = counts3 / sum(counts3);
% Calculate statistical measures
mean_intensity1 = mean(gray_cycle1(:));
mean_intensity2 = mean(gray_cycle2(:));
mean_intensity3 = mean(gray_cycle3(:));
std_intensity1 = std(double(gray_cycle1(:)));
std_intensity2 = std(double(gray_cycle2(:)));
std_intensity3 = std(double(gray_cycle3(:)));
% Display the results
fprintf('Cycle 1 - Mean Intensity: %.2f, Std Dev: %.2f\n', mean_intensity1,
std_intensity1);
fprintf('Cycle 2 - Mean Intensity: %.2f, Std Dev: %.2f\n', mean_intensity2,
std_intensity2);
fprintf('Cycle 3 - Mean Intensity: %.2f, Std Dev: %.2f\n', mean_intensity3,
std_intensity3);
% Plot histograms
figure;
subplot(3, 1, 1);
bar(binLocations1, counts1);
title('Histogram of Grayscale Intensities - Cycle 1');
xlabel('Grayscale Intensity');
ylabel('Normalized Frequency');
subplot(3, 1, 2);
bar(binLocations2, counts2);
title('Histogram of Grayscale Intensities - Cycle 2');
xlabel('Grayscale Intensity');
ylabel('Normalized Frequency');
subplot(3, 1, 3);
bar(binLocations3, counts3);
title('Histogram of Grayscale Intensities - Cycle 3');
xlabel('Grayscale Intensity');
ylabel('Normalized Frequency');
% Save the plot
saveas(gcf, 'color_intensity_histogram_analysis.png');
```